



1  
2  
3  
4  
5  
6  
7  
8  
9  
10  
11  
12  
13  
14  
15  
16  
17  
18  
19  
20  
21  
22  
23  
24  
25  
26  
27  
28  
29  
30  
31  
32  
33  
34  
35  
36  
37  
38

**A robust Upwind Mixed Hybrid Finite Element method for transport  
in variably saturated porous media**

Anis Younes<sup>1\*</sup>, Hussein Hoteit<sup>2</sup>, Rainer Helmig<sup>3</sup>, Marwan Fahs<sup>1</sup>

<sup>1</sup> Institut Terre et Environnement de Strasbourg, Université de Strasbourg, CNRS, ENGEES, UMR 7063, 67084  
Strasbourg, France

<sup>2</sup> Physical Science and Engineering Division, King Abdullah University of Science and Technology (KAUST),  
Thuwal, Saudi Arabia

<sup>3</sup> Institute for Modelling Hydraulic and Environmental Systems, University of Stuttgart, Pfaffenwaldring 61,  
70569 Stuttgart, Germany

*Submitted to Hydrology and Earth System Sciences (HESS)*

Contact author: Anis Younes

E-mail: [younes@unistra.fr](mailto:younes@unistra.fr)



39 **Abstract**

40 The Mixed Finite Element (MFE) method is well adapted for the simulation of fluid flow in  
41 heterogeneous porous media. However, when employed for the transport equation, it can  
42 generate solutions with strong unphysical oscillations because of the hyperbolic nature of  
43 advection. In this work, a robust upwind MFE scheme is proposed to avoid such unphysical  
44 oscillations. The new scheme is a combination of the upwind edge/face centred Finite Volume  
45 (FV) method with the hybrid formulation of the MFE method. The scheme ensures continuity  
46 of both advective and dispersive fluxes between adjacent elements and allows to maintain the  
47 time derivative continuous, which permits employment of high order time integration  
48 methods via the Method of Lines (MOL).

49 Numerical simulations are performed in both saturated and unsaturated porous media to  
50 investigate the robustness of the new upwind-MFE scheme. Results show that, contrarily to  
51 the standard scheme, the upwind-MFE method generates stable solutions without under and  
52 overshoots. The simulation of contaminant transport into a variably saturated porous medium  
53 highlights the robustness of the proposed upwind scheme when combined with the MOL for  
54 solving nonlinear problems.

55

56 **Keywords:**

57 Hybrid Mixed Finite Element, upwind scheme, advection-dispersion transport, numerical  
58 oscillations, Method of Lines.

59

60



## 61 **1. Introduction**

62 The Mixed Finite Element (MFE) method (Raviart and Thomas, 1977; Brezzi *et al.*, 1985;  
63 Chavent and Jaffré, 1986; Brezzi and Fortin, 1991, Younes *et al.*, 2010) is known to be a  
64 robust numerical scheme for solving elliptic diffusion problems such as the fluid flow in  
65 heterogeneous porous media. Indeed, the method combines advantages of the finite volumes,  
66 by ensuring local mass conservation and continuity of fluxes between adjacent cells, and  
67 advantages of finite elements by easily handling heterogeneous domains with discontinuous  
68 parameter distributions and unstructured meshes. As a consequence, the MFE method has  
69 been largely used for flow in porous media (see, for instance, the review of Younes *et al.*  
70 (2010) and references therein). The hybridization technique has been largely used with the  
71 MFE method to improve its efficiency (Chavent and Roberts, 1991; Traverso *et al.* 2013).  
72 Indeed, this technique allows to reduce the total number of unknowns and produces a final  
73 system with a symmetric positive definite matrix. The unknowns with the hybrid-MFE  
74 method are the Lagrange multipliers which correspond to the traces of the scalar variable at  
75 edges/faces (Chavent and Jaffré, 1986).

76 When applied to transient diffusion equations with small time steps, the hybrid-MFE method  
77 can produce solutions with small unphysical over and undershoots (Hoteit *et al.*, 2002a,  
78 2002b; Mazzia, 2008). A lumped formulation of the hybrid-MFE method was developed by  
79 Younes *et al.* (2006) to improve its monotonicity and reduce nonphysical oscillations. The  
80 lumped formulation ensures that the maximum principle is respected for parabolic diffusion  
81 equations on acute triangulations (Younes *et al.*, 2006). For more general 2D and 3D element  
82 shapes, the lumping procedure allows to significantly improve the monotonous character of  
83 the hybrid-MFE solution (Younes *et al.*, 2006; Koohbor *et al.*, 2020). As an illustration, the  
84 lumped formulation was shown to be more efficient and more robust than the standard hybrid  
85 formulation for the simulation of the challenging nonlinear problem of water infiltration into



86 an initially dry soil (Belfort *et al.*, 2009). The lumped formulation has recently been used for  
87 flow discretization in the case of density driven flow in saturated-unsaturated porous media  
88 (Younes *et al.*, 2022).

89 However, the MFE method remains little used for the discretization of the full transport  
90 equation. Indeed, when employed to the advection-dispersion equation, the MFE method can  
91 generate solutions with strong numerical instabilities in the case of advection-dominated  
92 transport because of the hyperbolic nature of the advection operator. To avoid these  
93 instabilities, one of the most popular and easiest ways is to use an upwind scheme. Indeed,  
94 although upwind schemes introduce some numerical diffusion leading to an artificial  
95 smearing of the numerical solution, they avoid unphysical oscillations and remain useful,  
96 especially for large domains and regional field simulations. In the literature, some upwind  
97 mixed finite element schemes have been employed to improve the robustness of the MFE  
98 method for advection-dominated problems (Dawson, 1998; Dawson and Aizinger, 1999;  
99 Radu *et al.*, 2011; Vohralik, 2007; Brunner *et al.*, 2014).

100 The main idea of an upwind scheme for an element  $E$ , is to calculate the mass flux exchanged  
101 with its adjacent element  $E'$  using the concentration from  $E$  in the case of an outflow and the  
102 concentration from  $E'$  in the case of an inflow. However, this idea cannot be applied as such  
103 with the hybrid-MFE method since the hybridization procedure requires to express the flux at  
104 the element interface as only a function of variables at the element  $E$  (and not  $E'$ ). To  
105 overcome this difficulty, Radu *et al.* (2011), and Brunner *et al.* (2014) proposed an upwind  
106 MFE method where, in the case of an inflow, the concentration at the adjacent element  $E'$  is  
107 replaced by an approximation using the concentration at  $E$  and the trace of concentration at  
108 the interface  $\partial_{EE'}$  by assuming that the edge concentration is the mean of the concentrations in  
109  $E$  and  $E'$ . However, this assumption cannot be verified for a general configuration.



110 Furthermore, with such an assumption, each of the advective and dispersive fluxes is  
111 discontinuous at the element interfaces, and continuity is only fulfilled for the total flux.

112 In this work, a new upwind-MFE method is proposed for solving the full transport equation  
113 without requiring any approximation of the upwind concentration. The new scheme is a  
114 combination of the upwind edge/face centered finite volume (FV) scheme with the lumped  
115 formulation of the MFE method. It guarantees continuity of both advective and dispersive  
116 fluxes at element interfaces. Further, the new upwind-MFE scheme maintains the time  
117 derivative continuous and thus, allows to employ high order time integration methods via the  
118 method of lines (MOL), which was shown to be very efficient for solving nonlinear problems  
119 (see, for instance, Fahs *et al.* (2009) and Younes *et al.* (2009)).

120 This article is structured as follows. In section 2, we recall the hybrid-MFE method for the  
121 discretization of the transport equation. In section 3, we introduce the new upwind-MFE  
122 method based on the combination of the upwind edge/face FV scheme with the lumped  
123 formulation of the MFE method. In section 4, numerical experiments are performed for  
124 transport in saturated and unsaturated porous media to investigate the robustness of the new  
125 developed upwind-MFE scheme. Some conclusions are given in the last section of the article.

## 126 **2. The hybrid-MFE method for the advection-dispersion equation**

127 The water mass conservation in variably saturated porous media can be written as follows:

$$128 \quad \frac{\partial \theta}{\partial t} + \nabla \cdot \mathbf{q} = 0 \quad (1)$$

129 where  $\theta$  is the water content [ $L^3L^{-3}$ ],  $t$  is the time [T], and  $\mathbf{q}$  is the Darcy velocity [ $LT^{-1}$ ].

130 The velocity  $\mathbf{q}$  is obtained by solving Richards' equation using the hybrid-MFE method. For  
131 a two-dimensional domain with a triangular mesh,  $\mathbf{q}$  is approximated inside each triangle  $E$   
132 using the lowest-order Raviart-Thomas (RT0) vectorial basis functions  $\mathbf{w}_j^E$ :

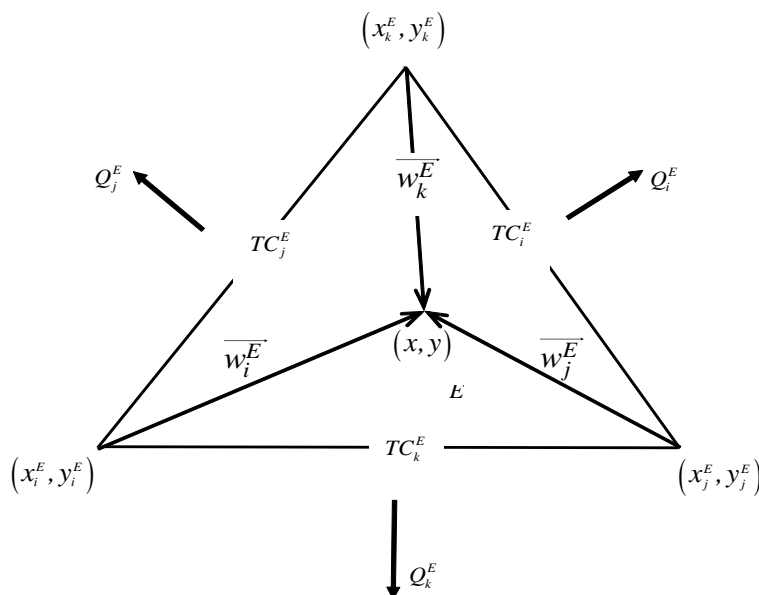


133 
$$\mathbf{q} = \sum_{j=1}^3 Q_j^E \mathbf{w}_j^E \quad (2)$$

134 where  $Q_j^E$  is the water flux across the edge  $E_j$  of  $E$  (see Figure 1) and  $\mathbf{w}_j^E = \frac{1}{2|E|} \begin{pmatrix} x - x_j^E \\ y - y_j^E \end{pmatrix}$

135 is the typical RT0 basis functions (Younes *et al.*, 1999) with  $(x_j^E, y_j^E)$  the coordinates of the

136 node  $j$  opposite to the edge  $E_j$  of  $E$  and  $|E|$ , the area of  $E$ .



137

138 Figure 1: Vectorial basis functions for the MFE method.

139

140 The mass conservation of the contaminant in variably saturated porous media is:

141 
$$\frac{\partial(\theta C)}{\partial t} + \nabla \cdot (\mathbf{q}C) + \nabla \cdot \tilde{\mathbf{q}}_d = 0 \quad (3)$$

142 where  $C$  is the normalized concentration [-],  $\mathbf{q}C$  is the advective flux and  $\tilde{\mathbf{q}}_d$  is the

143 dispersive flux given by:

144 
$$\tilde{\mathbf{q}}_d = -\mathbf{D}\nabla C \quad (4)$$



145 with  $\mathbf{D}$ , the dispersion tensor, expressed by:

$$146 \quad \mathbf{D} = D_m \mathbf{I} + (\alpha_L - \alpha_T) \mathbf{q} \otimes \mathbf{q} / |\mathbf{q}| + \alpha_T |\mathbf{q}| \mathbf{I} \quad (5)$$

147 in which  $\alpha_L$  and  $\alpha_T$  are the longitudinal and transverse dispersivities [L],  $D_m$  is the pore  
 148 water diffusion coefficient [ $L^2 T^{-1}$ ] and  $\mathbf{I}$  is the unit tensor.

149 Substituting Eq. (1) into Eq. (3) yields the following advection-dispersion equation:

$$150 \quad \theta \frac{\partial C}{\partial t} + \nabla \cdot (\mathbf{q} C + \tilde{\mathbf{q}}_d) - C \nabla \cdot \mathbf{q} = 0 \quad (6)$$

151 To apply the hybrid-MFE method to the transport Eq. (6), we approximate the dispersive flux  
 152  $\tilde{\mathbf{q}}_d$  with RT0 vectorial basis functions as:

$$153 \quad \tilde{\mathbf{q}}_d = \sum_{j=1}^3 \tilde{Q}_j^{d,E} \mathbf{w}_j^E \quad (7)$$

154 where  $\tilde{Q}_j^{d,E} = \int_{E_j} \tilde{\mathbf{q}}_d \cdot \boldsymbol{\eta}_j^E$  is the dispersive flux across the edge  $E_j$  of the element  $E$  and  $\boldsymbol{\eta}_j^E$  is  
 155 the outward unit normal vector to the edge  $E_j$ .

156 The variational formulation of Eq. (4) using the test function  $\mathbf{w}_i^E$  yields:

$$157 \quad \int_E \mathbf{D}^{-1} \tilde{\mathbf{q}}_d \cdot \mathbf{w}_i^E = \int_E C \nabla \cdot \mathbf{w}_i^E - \sum_j \int_{E_j} C \mathbf{w}_i^E \cdot \boldsymbol{\eta}_j^E \quad (8)$$

158 Substituting Eq. (7) into Eq. (8) and using properties of the basis functions  $\mathbf{w}_j^E$  give

$$159 \quad \sum_j \tilde{Q}_j^{d,E} \int_E (\mathbf{D}_E^{-1} \mathbf{w}_j^E) \cdot \mathbf{w}_i^E = \frac{1}{|E|} \int_E C - \frac{1}{|E_i|} \int_{E_i} C \quad (9)$$

$$= C_E - TC_i^E$$

160 in which,  $\mathbf{D}_E$  is the local dispersion tensor at the element  $E$ ,  $C_E$  is the mean concentration at  
 161  $E$  and  $TC_i^E$  is the edge (trace) concentration (Lagrange multiplier) at the edge  $E_i$ .

162 Denoting the local matrix  $\tilde{B}_{i,j}^{-1,E} = \int_E (\mathbf{D}_E^{-1} \mathbf{w}_j^E) \cdot \mathbf{w}_i^E$ , the inversion of the system of Eq. (9) gives

163 the expression for the dispersive flux  $\tilde{Q}_i^{d,E}$ :



$$164 \quad \tilde{Q}_i^{d,E} = \sum_j \tilde{B}_{i,j}^{-1,E} (C_E - TC_j^E) \quad (10)$$

165 Besides, the integration of the mass conservation Eq. (6) over the element  $E$  writes

$$166 \quad \int_E \theta \frac{\partial C}{\partial t} + \int_E \nabla \cdot (\mathbf{q}C) + \int_E \nabla \cdot \tilde{\mathbf{q}}_d - \int_E C \nabla \cdot \mathbf{q} = 0 \quad (11)$$

167 which becomes, using Green's formula,

$$168 \quad \theta_E |E| \frac{\partial C_E}{\partial t} + \sum_i \int_{E_i} C \mathbf{q} \cdot \boldsymbol{\eta}_i^E + \sum_i \int_{E_i} \tilde{\mathbf{q}}_d \cdot \boldsymbol{\eta}_i^E - \int_E C \nabla \cdot \mathbf{q} = 0 \quad (12)$$

169 where  $\theta_E$  is the water content of the element  $E$ .

170 Substituting Eq. (2) into Eq. (12) yields

$$171 \quad \theta_E |E| \frac{\partial C_E}{\partial t} + \sum_i \underbrace{(\tilde{Q}_i^{a,E} + \tilde{Q}_i^{d,E})}_{\tilde{Q}_i^{t,E}} - C_E \sum_i Q_i^E = 0 \quad (13)$$

172 in which  $\tilde{Q}_i^{t,E} = \tilde{Q}_i^{a,E} + \tilde{Q}_i^{d,E}$  is the total flux at the edge  $E_i$  with  $\tilde{Q}_i^{a,E}$  the advective flux given  
 173 by  $\tilde{Q}_i^{a,E} = Q_i^E TC_i^E$  and  $\tilde{Q}_i^{d,E}$  the dispersive flux given by Eq. (10).

174 The hybridization of the MFE method is performed in the following three steps:

175 1) The flux Eq. (10) is substituted into the mass conservation Eq. (13), which is then

176 discretized in time using the first-order implicit Euler scheme

$$177 \quad \theta_E \frac{|E|}{\Delta t} (C_E^{n+1} - C_E^n) + \sum_i Q_i^E TC_i^{E,n+1} - C_E^{n+1} \sum_i Q_i^E + \tilde{\alpha}^E C_E^{n+1} - \sum_i \tilde{\alpha}_i^E TC_i^{E,n+1} = 0 \quad (14)$$

178 in which  $\tilde{\alpha}_i^E = \sum_j \tilde{B}_{i,j}^{-1,E}$  and  $\tilde{\alpha}^E = \sum_i \tilde{\alpha}_i^E$ .

179 Hence, the mean concentration at the new time level  $C_E^{n+1}$  can be expressed as a function

180 of  $TC_i^{E,n+1}$ , the concentration at the edges of  $E$ , as follows:

$$181 \quad C_E^{n+1} = \frac{1}{\beta_E} \sum_i (\tilde{\alpha}_i^E - Q_i^E) TC_i^{E,n+1} + \frac{\lambda_E}{\beta_E} C_E^n \quad (15)$$





182 in which  $\lambda_E = \theta_E \frac{|E|}{\Delta t}$  and  $\beta_E = \left( \lambda_E + \tilde{\alpha}^E - \sum_i Q_i^E \right)$ .

183 2) The mean concentration given by Eq. (15) is then substituted into the flux Eq. (10), which

184 allows expressing the dispersive flux  $\tilde{Q}_i^{d,E}$  as only a function of the traces of concentration

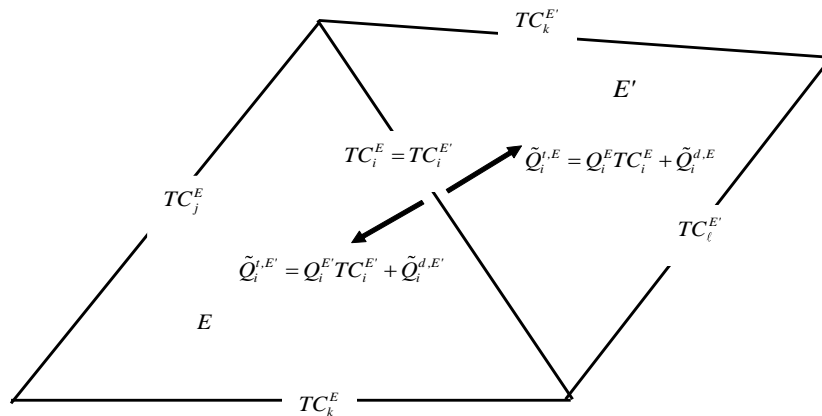
185 at edges  $TC_i^{E,n+1}$ :

$$186 \quad \tilde{Q}_i^{d,E} = \sum_j \left( \frac{\tilde{\alpha}_i^E}{\beta_E} (\tilde{\alpha}_j^E - Q_j^E) - \tilde{B}_{i,j}^{-1,E} \right) TC_j^{E,n+1} + \frac{\lambda_E}{\beta_E} \tilde{\alpha}_i^E C_E^n \quad (16)$$

187 3) Finally, the system to be solved is obtained by imposing the continuity of the total flux

188 ( $\tilde{Q}_i^{t,E} + \tilde{Q}_i^{t,E'} = 0$ ) as well as the continuity of the trace of concentration ( $TC_i^{E,n+1} = TC_i^{E',n+1}$ )

189 at the edge  $i$  between the two elements  $E$  and  $E'$  (Figure 2).



190

191 Figure 2: Continuity of concentration and total flux between adjacent elements with the  
 192 hybrid-MFE method.

193 Note that the advective flux  $\tilde{Q}_i^{a,E}$  is continuous between  $E$  and  $E'$  because of the continuity of

194 the water flux and the continuity of the trace of concentration at the interface. Thus, for the

195 continuity of the total flux ( $\tilde{Q}_i^{t,E} + \tilde{Q}_i^{t,E'} = 0$ ), it is required that the dispersive flux is

196 continuous:



$$197 \quad \tilde{Q}_i^{a,E} + \tilde{Q}_i^{a,E'} = (Q_i^E + Q_i^{E'}) TC_i^E + \tilde{Q}_i^{d,E} + \tilde{Q}_i^{d,E'} = \tilde{Q}_i^{d,E} + \tilde{Q}_i^{d,E'} = 0 \quad (17)$$

198 Using Eq. (16), we obtain:

$$199 \quad \sum_j \left( \tilde{B}_{i,j}^{E',-1} - \frac{\tilde{\alpha}_i^E}{\beta_E} (\tilde{\alpha}_j^E - Q_j^E) \right) TC_j^{E,n+1} + \sum_j \left( \tilde{B}_{i,j}^{E',-1} - \frac{\tilde{\alpha}_i^{E'}}{\beta_{E'}} (\tilde{\alpha}_j^{E'} - Q_j^{E'}) \right) TC_j^{E',n+1} \\ = \frac{\lambda_E}{\beta_E} \tilde{\alpha}_i^E C_E^n + \frac{\lambda_{E'}}{\beta_{E'}} \tilde{\alpha}_i^{E'} C_{E'}^n \quad (18)$$

200 This equation is written for all mesh edges, and the resulting equations form the final system  
 201 to be solved for the traces of concentration at edges  $TC_i^{E,n+1}$  as unknowns.

202 Note that the hybrid-MFE Eqs (18), obtained by approximating the dispersive flux with RT0  
 203 basis functions, is equivalent to the new MFE method proposed in Radu *et al.* (2011).

204

### 205 3. The upwind-MFE method for the transport equation

206 In the case of advection-dominated transport, solving the hybrid-MFE Eq. (18) can yield  
 207 solutions with strong instabilities. A common way to avoid such instabilities is to use an  
 208 upwind scheme for the advective flux. Thus, for an element  $E$ , the advective flux

209  $\tilde{Q}_i^{a,E} = Q_i^E TC_i^E$  at the edge  $i$  (common with the element  $E$ ), has to be calculated using either

210 the concentration from  $E$  (if  $Q_i^E > 0$ ) or the concentration from  $E'$  (if  $Q_i^E < 0$ ). To this aim,

211 Radu *et al.* (2011) suggested replacing the advective flux  $\tilde{Q}_i^{a,E} = Q_i^E TC_i^E$  at the interface by:

$$212 \quad \tilde{Q}_i^{a,E} = \begin{cases} Q_i^E C^E & \text{if } Q_i^E > 0 \\ Q_i^E C^{E'} & \text{if } Q_i^E < 0 \end{cases} \quad (19)$$

213 Thus, the advective term is now calculated using the upwind mean concentration, which can  
 214 be that of the element  $E$  or of its adjacent element  $E'$ .

215 The advective flux of Eq. (19) is rewritten in the following condensed form

$$216 \quad \tilde{Q}_i^{a,E} = Q_i^E \left( \tau_i^E C^E + (1 - \tau_i^E) C^{E'} \right) \quad (20)$$



217 with  $\tau_i^E = 1$  for an outflow ( $Q_i^E > 0$ ) and  $\tau_i^E = 0$  for an inflow ( $Q_i^E < 0$ ).

218 However, this expression is incompatible with the hybridization procedure. Indeed, if we  
 219 replace, in the Eq. (14), the advective term  $Q_i^E TC_i^E$  by Eq. (20), the latter will contain both  
 220  $C^E$  and  $C^{E'}$ . Thus, the first step of the hybridization procedure cannot allow expressing  
 221  $C_E^{n+1}$  as only a function of  $TC_i^{E,n+1}$  as in the Eq. (15).

222 To avoid this difficulty, Radu *et al.* (2011) suggested replacing,  $C^{E'}$  by the following  
 223 expression:

$$224 \quad C^{E'} \simeq 2TC_i^E - C^E \quad (21)$$

225 This approximation is based on the assumption that  $TC_i^E \simeq (C^E + C^{E'})/2$ .

226 Plugging Eq. (21) into Eq. (20), the advective flux  $\tilde{Q}_i^{a,E}$  depends only on the variables of the  
 227 element  $E$  (mean concentration  $C^E$  and edge concentration  $TC_i^E$ ):

$$228 \quad \tilde{Q}_i^{a,E} = Q_i^E \left( \tau_i^E C^E - (1 - \tau_i^E) C^E + 2(1 - \tau_i^E) TC_i^E \right) \quad (22)$$

229 Eq. (22) can then be used to replace the advective term  $Q_i^E TC_i^E$  in Eq. (14), and thus the  
 230 hybridization procedure allows to express  $C_E^{n+1}$  as a function of  $TC_i^{E,n+1}$  as in the Eq. (15).

231 Then, the obtained expression of  $C_E^{n+1}$  is substituted into the dispersive flux Eq. (10), and the  
 232 final system is then obtained by prescribing continuity of the total flux ( $\tilde{Q}_i^{a,E} + \tilde{Q}_i^{d,E'} = 0$ ) at the  
 233 interface between  $E$  and  $E'$ .

234 Note that Eq. (21) can be a rough approximation, especially in the case of heterogeneous  
 235 domains where dispersion can vary with several orders of magnitudes between the elements  $E$   
 236 and  $E'$ . Furthermore, the advective flux is not uniquely defined at the interface and can be  
 237 different for the adjacent elements  $E$  and  $E'$ . For instance, in the case of  $Q_i^E = Q > 0$ , the  
 238 advective flux leaving the element  $E$  is  $\tilde{Q}_i^{a,E} = QC^E$ , whereas the flux entering the element  $E'$



239 is  $\tilde{Q}_i^{a,E'} = Q(2TC_i^E - C^{E'})$  which could be different as  $TC_i^E$  is not necessarily the mean of  $C^E$   
 240 and  $C^{E'}$ . In this situation, because of the discontinuity of the advective flux, the dispersive  
 241 flux will not be continuous at the interface since the continuity is prescribed only for the total  
 242 flux.

243 To avoid the rough approximation (21), we develop hereafter a new upwind-MFE scheme  
 244 where the advection term is calculated using upwind edge concentration in the element  $E$ . The  
 245 idea of the scheme is to combine the upwind edge finite volume method with the lumped  
 246 formulation of the MFE method. The scheme is elaborated in the following four steps:

247 1) In a first step, the steady-state dispersive transport (i.e. the first, second and fourth terms  
 248 are removed from Eq. (12)) yields:

$$249 \quad \sum_i \tilde{Q}_i^{d,E} = 0 \quad (23)$$

250 where  $\tilde{Q}_i^{d,E}$  corresponds to the steady-state dispersive flux across the edge  $E_i$ .

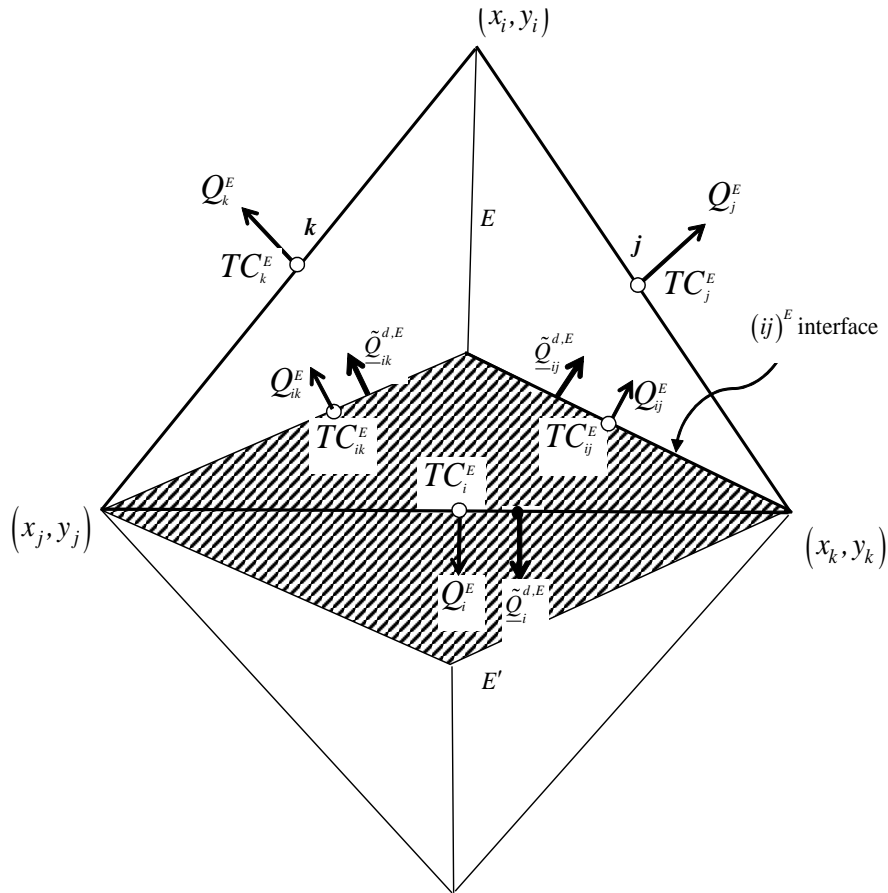
251 Therefore, the mean concentration in Eq. (15) becomes

$$252 \quad C_E = \sum_i \frac{\tilde{\alpha}_i^E}{\tilde{\alpha}^E} TC_i^E \quad (24)$$

253 and the steady-state dispersive flux, given by Eq. (16), becomes

$$254 \quad \tilde{Q}_i^{d,E} = \sum_j \left( \frac{\tilde{\alpha}_i^E \tilde{\alpha}_j^E}{\tilde{\alpha}^E} - \tilde{B}_{i,j}^{-1,E} \right) TC_j^E \quad (25)$$

255 2) In a second step, a simplex region  $S_i^E$  is constructed around each edge  $i$  by joining the two  
 256 nodes of edge  $i$  to the element center  $\mathbf{x}_E$  (Figure 3).



257

258 Figure 3: The lumping region  $R_i$  associated with the edge  $i$ , sharing the elements  $E$  and

259

$E'$  and formed by the two simplex regions  $S_i^E$  and  $S_i^{E'}$ .

260

The domain is now partitioned into lumping regions  $R_i$  (hatched area in Figure 3) assigned

261

to the edge  $i$ , formed by the two simplex regions  $S_i^E$  and  $S_i^{E'}$  for an inner edge  $i$  and by the

262

sole simplex region  $S_i^E$  for a boundary edge. The simplex region  $S_i^E$  is defined by joining

263

the centre of  $E$  with the nodes  $j$  and  $k$  forming the edge  $i$ .

264

3) In a third step, the integration of the mass conservation Eq. (6) over the lumping region  $R_i$

265

yields:



$$266 \quad \int_{R_i} \theta \frac{\partial C}{\partial t} + \int_{R_i} \nabla \cdot (\mathbf{q}C) + \int_{R_i} \nabla \cdot \tilde{\mathbf{q}}_d - \int_{R_i} C \nabla \cdot \mathbf{q} = 0 \quad (26)$$

267 Associating the concentration  $TC_i^E$  to  $R_i$  yields (see Figure 3 for notations)

$$268 \quad \left\{ \frac{|E|}{3} \theta_E \frac{\partial TC_i^E}{\partial t} + Q_{ij}^E TC_{ij}^E + Q_{ik}^E TC_{ik}^E + \tilde{Q}_{ij}^{d,E} + \tilde{Q}_{ik}^{d,E} - TC_i^E (Q_{ij}^E + Q_{ik}^E) \right\} + \{ \} ' = 0 \quad (27)$$

269 in which  $Q_{ij}^E$ ,  $\tilde{Q}_{ij}^{d,E}$  and  $TC_{ij}^E$  are respectively the water flux, the dispersive flux and the  
 270 concentration at the interior interface  $(ij)^E$  between the simplex regions  $S_i^E$  and  $S_j^E$ .

271 The interior flux  $Q_{ij}^E$  is evaluated using the RT0 approximation of the velocity given by  
 272 Eq. (2), which yields

$$273 \quad Q_{ij}^E = \frac{1}{3} (Q_j^E - Q_i^E) \quad (28)$$

274 Besides, applying the steady-state dispersive transport Eq. (23) on the simplex region  $S_i^E$   
 275 yields:

$$276 \quad \tilde{Q}_{ij}^{d,E} + \tilde{Q}_{ik}^{d,E} + \tilde{Q}_i^{d,E} = 0 \quad (29)$$

277 Hence, Eq. (27) becomes

$$278 \quad \left\{ \frac{|E|}{3} \theta_E \frac{\partial TC_i^E}{\partial t} - \tilde{Q}_i^{d,E} + Q_{ij}^E TC_{ij}^E + Q_{ik}^E TC_{ik}^E - (Q_{ij}^E + Q_{ik}^E) TC_i^E \right\} + \{ \} ' = 0 \quad (30)$$

279 Using Eq. (25) and denoting  $\lambda_E = \theta_E \frac{|E|}{3}$ , we obtain

$$280 \quad \left\{ \lambda_E \frac{\partial TC_i^E}{\partial t} + \sum_j \left( \tilde{B}_{i,j}^{-1,E} - \frac{\tilde{\alpha}_i^E \tilde{\alpha}_j^E}{\tilde{\alpha}^E} \right) TC_j^E + Q_{ij}^E TC_{ij}^E + Q_{ik}^E TC_{ik}^E - (Q_{ij}^E + Q_{ik}^E) TC_i^E \right\} + \{ \} ' = 0 \quad (31)$$

281 4) In a fourth step, the interior concentration  $TC_{ij}^E$  at the interface between the simplex  
 282 regions  $S_i^E$  and  $S_j^E$  is calculated using an upwind scheme (See Figure 3) defined by:

$$283 \quad TC_{ij}^E = \tau_{ij}^E TC_i^E + (1 - \tau_{ij}^E) TC_j^E \quad (32)$$



284 with  $\tau_{ij}^E = 1$  if  $(Q_{ij}^E \geq 0)$ , else  $\tau_{ij}^E = 0$

285 Thus, the final system to solve becomes,

$$286 \left\{ \lambda_E \frac{\partial TC_i^E}{\partial t} + \sum_j \left( \tilde{B}_{i,j}^{-1,E} - \frac{\tilde{\alpha}_i^E \tilde{\alpha}_j^E}{\tilde{\alpha}^E} \right) TC_j^E + Q_{ij}^E (1 - \tau_{ij}^E) (TC_j^E - TC_i^E) + Q_{ik}^E (1 - \tau_{ik}^E) (TC_k^E - TC_i^E) \right\} \\ + \{ \} ' = 0$$

287 (33)

288 Note that contrarily to the standard hybrid-MFE scheme, where the discretization of the  
 289 temporal derivative performed in Eq. (14) was necessary to obtain the final system given  
 290 by Eq. (18), the new scheme given by Eq. (33) keeps the time derivative continuous which  
 291 allows the use of efficient high order temporal discretization methods via the MOL.

292 In the case of a first-order Euler implicit time discretization, Eq. (33) becomes

$$293 \left\{ \sum_j \left( \tilde{B}_{i,j}^{-1,E} - \frac{\tilde{\alpha}_i^E \tilde{\alpha}_j^E}{\tilde{\alpha}^E} \right) TC_j^{E,n+1} + \lambda_E TC_i^{E,n+1} + Q_{ij}^E (1 - \tau_{ij}^E) (TC_j^{E,n+1} - TC_i^{E,n+1}) \right\} + \{ \} ' = 0 \quad (34) \\ \left\{ + Q_{ik}^E (1 - \tau_{ik}^E) (TC_k^{E,n+1} - TC_i^{E,n+1}) - \lambda_E TC_i^{E,n} \right\}$$

294 where  $\lambda_E = \theta_E \frac{|E|}{3\Delta t}$ .

295 Eq. (34) expresses the total exchange between  $E$  and  $E'$  and therefore reflects the continuity  
 296 of the total (advection + dispersion) flux between them. With this formulation, both advective  
 297 and dispersive fluxes are continuous between the adjacent elements  $E$  and  $E'$ . Indeed, the  
 298 advective flux, calculated using the upwind edge concentration, is uniquely defined at the  
 299 interface of the lumping region and is therefore continuous. As a consequence, the dispersive  
 300 flux is also continuous between  $E$  and  $E'$  since the total flux is continuous at the interface  
 301 between them.

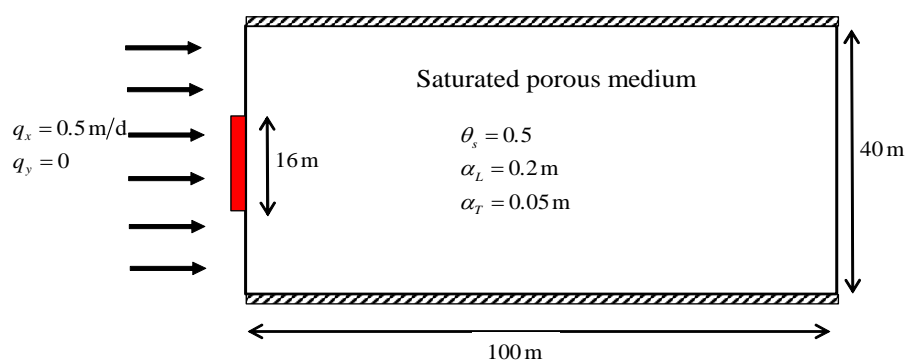


## 302 4. Numerical Experiments

303 In this section, a first test case dealing with transport in saturated porous media is simulated  
304 with the standard hybrid-MFE and the new upwind-MFE schemes. The results are compared  
305 against an analytical solution in order to validate the new developed scheme and to show its  
306 robustness for solving advection-dominated transport problems compared to the standard one.  
307 The second test case deals with transport in the unsaturated zone and aims to investigate the  
308 robustness of the new scheme when combined with the MOL for solving highly nonlinear  
309 problems.

### 310 4.1 Transport in saturated porous media: comparison against a 2D analytical solution

311 The hybrid and upwind MFE formulations are compared against the analytical solution  
312 developed by Leij and Dane (1990) for a simplified 2D transport problem (Figure 4). The  
313 latter deals with the contamination from the left boundary of a 2D rectangular domain of  
314 dimension  $(0,100) \times (0,40)$ .



315

316 Figure 4: Description of the problem of the contamination of a 2D saturated porous medium.

317 The boundary conditions for the transport are of Dirichlet type at the inflow (left vertical  
318 boundary), with





$$319 \quad C = \begin{cases} 0 & \text{for } x = 0 \text{ and } 0 \leq y < 12 \\ 1 & \text{for } x = 0 \text{ and } 12 \leq y \leq 28 \\ 0 & \text{for } x = 0 \text{ and } 28 < y \leq 40 \end{cases} \quad (35)$$

320 A zero diffusive flux is imposed at the right vertical outflow boundary. The top and bottom  
321 are no-flow boundaries. A uniform horizontal flow occurs from left to right with fluid velocity  
322  $V_x = 1.0$  m/day and  $V_y = 0$ . The longitudinal and transverse dispersivities are  $\alpha_L = 0.2m$  and  
323  $\alpha_T = 0.05m$ , respectively. The domain is discretized with a fine unstructured triangular mesh  
324 formed by 33216 elements, and the simulation is performed for a final simulation time  $T = 30$   
325 days using a fixed time step of 0.1 day.

326 The analytical solution of this test case for an infinite domain is given by Leij and Dane  
327 (1990):

$$328 \quad C(x, y, t) = \frac{x}{(16\pi\alpha_L)^{1/2}} \int_0^T \tau^{-3/2} \left\{ \operatorname{erf} \left[ \frac{y-12}{(4\alpha_T\tau)^{1/2}} \right] + \operatorname{erf} \left[ \frac{28-y}{(4\alpha_T\tau)^{1/2}} \right] \right\} \exp \left[ -\frac{(x-\tau)^2}{4\alpha_L\tau} \right] d\tau \quad (36)$$

$$329 \quad \text{with } \operatorname{erf}(x) = \frac{2}{\sqrt{\pi}} \int_0^x \exp(-\tau^2) d\tau.$$

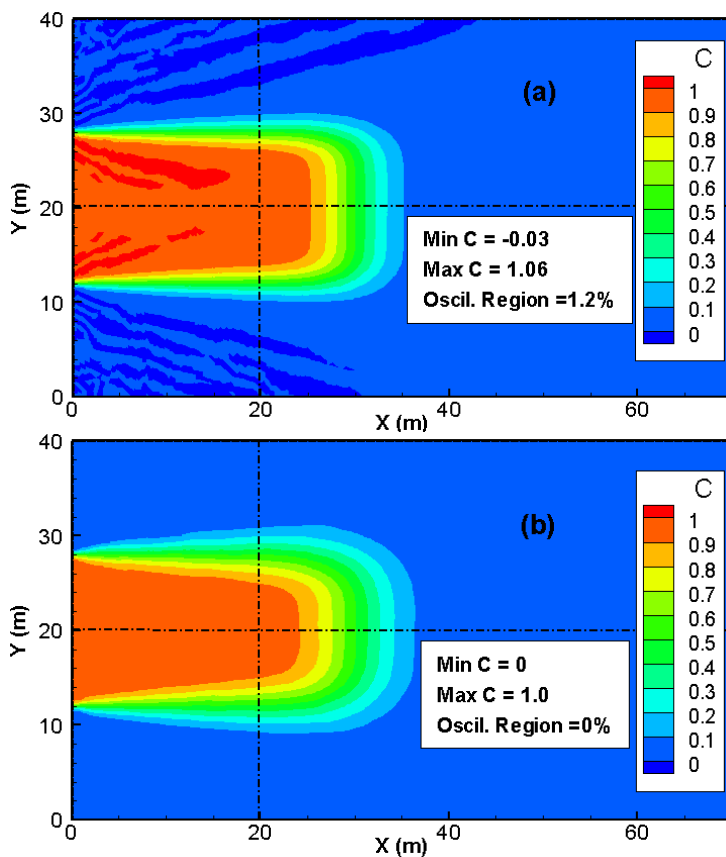
330

331 The final distributions of the concentration with both hybrid-MFE and upwind-MFE schemes  
332 are depicted in Figure 5. The hybrid-MFE scheme (Figure 5a) yields a solution with  
333 unphysical oscillations. Indeed, around 1.2 % of the contaminated region (*i.e.* the region with  
334  $|C| \geq 10^{-5}$ ) exhibits unphysical oscillations with 0.4 % of the contaminated region with  
335  $C \leq -10^{-3}$  and 0.8 % of the contaminated region with  $C \geq 1.001$ . These unphysical  
336 oscillations, although they seem moderate, can be dramatic, for instance, when dealing with  
337 reactive transport where some reactions occur only if the concentration exceeds a certain  
338 threshold. The solution obtained with the new upwind formulation (Figure 5b) is monotone  
339 (all concentrations are between 0 and 1) which is in agreement with the physics. However,  
340 these results come at the expense of some numerical diffusion added to the solution. To



341 appreciate the quality of both solutions and validate the upwind-MFE method, we compare  
342 the concentration profile of the two methods to the analytical solution of Leij and Dane (1990)  
343 for a horizontal section located at  $y = 20$  m and a vertical section located at  $x = 20$  m.

344



346

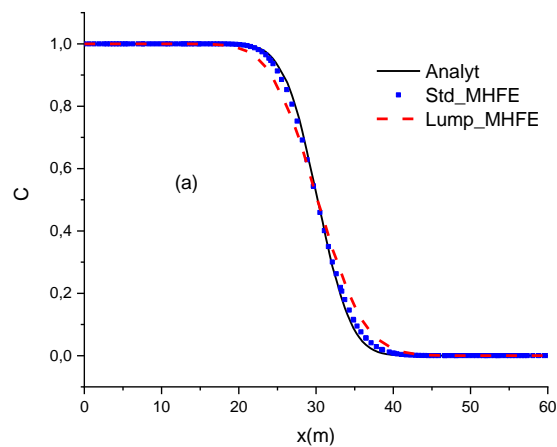
347 Figure 5: Concentration distribution with the hybrid-MFE and the upwind-MFE methods for  
348 the 2D saturated transport problem (only the region  $x \leq 70$  m is depicted).

349

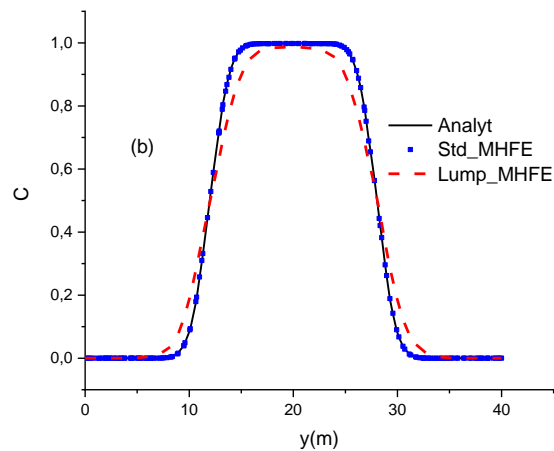
350 The results of figure 6 show that the solution of both hybrid-MFE and upwind-MFE methods  
351 are in very good agreement with the analytical solution, which validates the new upwind-  
352 MFE numerical model. Note, however, that a small numerical diffusion is observed with the  
353 upwind-MFE solution, which is especially visible in figure 6b. Indeed, for the simulated  
354 problem, the transverse dispersivity is much smaller than the longitudinal one, and, as a



355 consequence, the concentration front is sharper in the vertical section than in the horizontal  
356 one. This explains why the numerical diffusion generated by the upwind-MFE method is  
357 more pronounced in Figure 6b than in Figure 6a.  
358



359



360

361 Figure 6: Concentration profiles at  $y = 20\text{m}$  (a) and  $x = 20\text{m}$  (b) with the analytical, hybrid-  
362 MFE and upwind-MFE solutions.

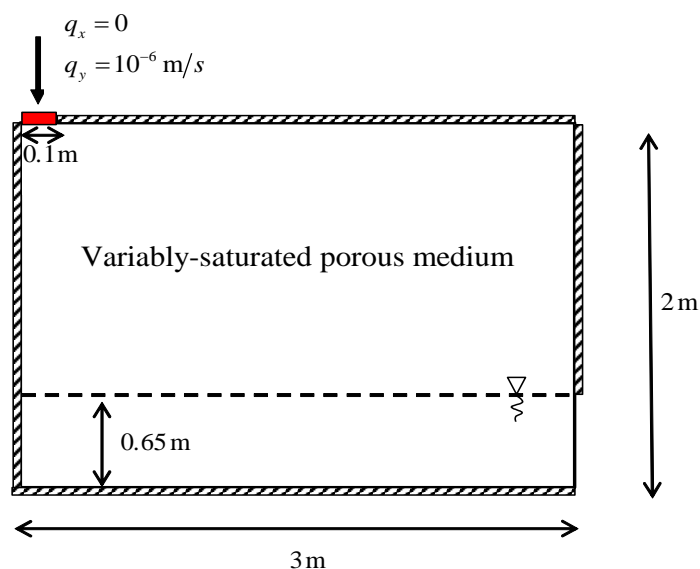
363



364 4.2 *Transport in a variably-saturated porous medium.*

365 In this test case, the developed upwind-MFE method is combined with the MOL for solving  
366 contaminant transport in a variably-saturated porous medium. The advection-dispersion  
367 equation is transformed to an Ordinary Differential Equation (ODE) using the new upwind-  
368 MFE formulation for the spatial discretization, whereas the time derivative is maintained  
369 continuous. Therefore, high-order time integration methods included in efficient ODE solvers  
370 can be employed. With these solvers, both the time step size and the order of the time  
371 integration can vary during the simulation to deliver accurate results in an acceptable  
372 computational time.

373 To investigate the robustness and efficiency of the combination of the developed upwind-  
374 MFE method with the MOL, we simulate in this section the problem of contaminant  
375 infiltration into a variably-saturated porous medium.



376

377 Figure 7: Description of the problem of contaminant infiltration into a 2D variably-saturated  
378 porous medium.

379



380 The domain (Figure 7) is a rectangular box of  $3\text{m} \times 2\text{m}$ , filled with sand, with an initial water  
 381 table at  $0.65\text{m}$  and hydrostatic pressure distribution. An infiltration of a tracer contaminant is  
 382 applied over the left-most  $0.1\text{m}$  of the surface with a constant flux of  $10^{-6}\text{ m/s}$ . The right  
 383 vertical side has a fixed head of  $0.65\text{m}$  below the water table and a no-flow boundary above it.  
 384 The left vertical side as well as the upper (except the infiltration zone) and bottom boundaries  
 385 are no-flow boundaries.

386 In this problem, the flow and transport are coupled by the velocity, which is obtained by  
 387 solving the following pressure-head form of the nonlinear Richards' equation:

$$388 \quad \left( c(h) + S_s \frac{\theta}{\theta_s} \right) \frac{\partial H}{\partial t} + \nabla \cdot \mathbf{q} = 0 \quad (31)$$

$$389 \quad \mathbf{q} = -k_r \mathbf{K} \nabla H \quad (32)$$

390 with  $S_s$  the specific mass storativity related to head changes [ $\text{L}^{-1}$ ],  $H = h + y$  the equivalent  
 391 freshwater head [ $\text{L}$ ],  $h = \frac{P}{\rho g}$  the pressure head,  $P$  the pressure [ $\text{Pa}$ ],  $\rho$  the fluid density  
 392 [ $\text{ML}^{-3}$ ],  $g$  the gravity acceleration [ $\text{LT}^{-2}$ ],  $y$  the upward vertical coordinate [ $\text{L}$ ],  $c(h)$  the  
 393 specific moisture capacity [ $\text{L}^{-1}$ ],  $\theta_s$  the saturated water content [ $\text{L}^3\text{L}^{-3}$ ],  $\mathbf{q}$  the Darcy velocity  
 394 [ $\text{LT}^{-1}$ ],  $\mathbf{K} = \frac{\rho g}{\mu} \mathbf{k}$  the hydraulic conductivity [ $\text{LT}^{-1}$ ],  $\mathbf{k}$  the permeability [ $\text{L}^2$ ],  $\mu$  the fluid  
 395 dynamic viscosity [ $\text{ML}^{-1}\text{T}^{-1}$ ] and  $k_r$  the relative conductivity [-].

396 We use the standard van Genuchten (1980) model for the relationship between water content  
 397 and pressure head:

$$398 \quad S_e = \frac{\theta(h) - \theta_r}{\theta_s - \theta_r} = \begin{cases} \frac{1}{(1 + |\alpha h|^n)^m} & h < 0 \\ 1 & h \geq 0 \end{cases} \quad (33)$$



399 where  $\alpha$  [ $L^{-1}$ ] and  $n$  [-] are the van Genuchten parameters,  $m = 1 - 1/n$ ,  $S_e$  [-] is the effective  
 400 saturation and  $\theta_r$  [-] is the residual water content. The conductivity-saturation relationship is  
 401 derived from the Mualem (1976) model:

$$402 \quad k_r = S_e^{1/2} \left[ 1 - \left( 1 - S_e^{1/m} \right)^m \right]^2 \quad (34)$$

403 The material properties of the test problem are given in Table 1.

| Parameters                   |            |
|------------------------------|------------|
| $\theta_r$                   | 0.01       |
| $\theta_s$                   | 0.3        |
| $\alpha$ ( $cm^{-1}$ )       | 0.033      |
| $n$                          | 4.1        |
| $K$ ( $cm s^{-1}$ )          | $10^{-2}$  |
| $S_s$ ( $cm^{-1}$ )          | $10^{-10}$ |
| $D_m$ ( $m^2 s^{-1}$ )       | $10^{-9}$  |
| $\rho$ ( $kg m^{-3}$ )       | 1000       |
| $\mu$ ( $kg m^{-1} s^{-1}$ ) | 0.001      |

404

405 Table 1: Parameters for the problem of infiltration into a 2D variably-saturated porous  
 406 medium.

407

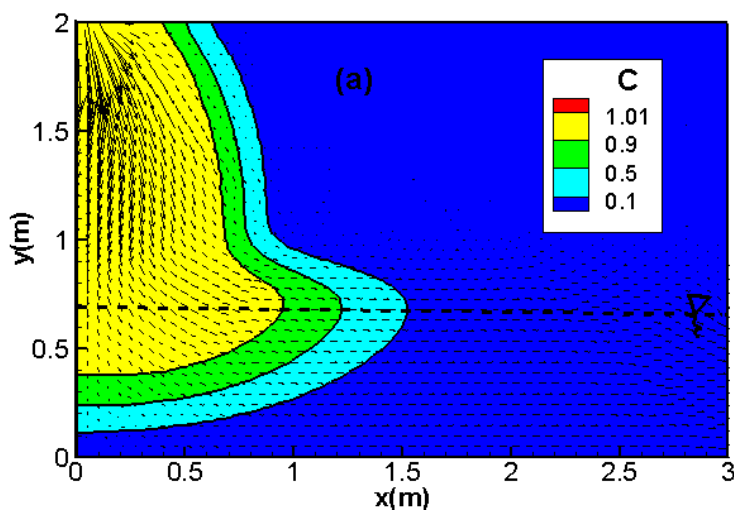
408 The simulation is performed for 80 hours using a triangular mesh formed by 4273 triangular  
 409 elements. Two test cases are investigated. In the first test case, the longitudinal and transverse  
 410 dispersivities are  $\alpha_L = 0.03m$  and  $\alpha_T = 0.003m$ , respectively. The second test case is less  
 411 diffusive with  $\alpha_L = 0.01m$  and  $\alpha_T = 0.001m$ .

412 The coupled nonlinear flow-transport system is solved using the MOL, which allows the use  
 413 of efficient high-order time integration methods, for both the hybrid-MFE and the upwind-  
 414 MFE schemes. To this aim, a hybrid-MFE formulation with continuous time derivative was

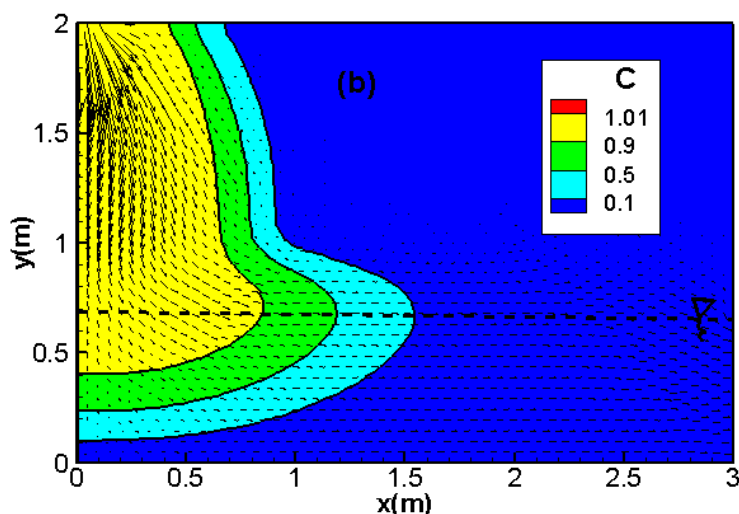


415 developed by extending the lumping procedure, developed in Younes *et al.* (2006) for the  
416 flow equation, to the advection-dispersion transport Eq. (6).

417 The results of the hybrid-MFE and the upwind-MFE methods are depicted in Figure 8 for the  
418 first test case involving high dispersion. Good agreement can be observed between the results  
419 of the hybrid-MFE (Figure 8a) and upwind-MFE (Figure 8b) schemes when combined with  
420 the MOL. In these figures, the contaminant progresses essentially vertically through the  
421 unsaturated zone of the soil. When the saturated zone is reached, the contaminant progresses  
422 horizontally and remains close to the water table. Note that the results of both schemes are  
423 stable and free from unphysical oscillations (Figures 8a and 8b).



424

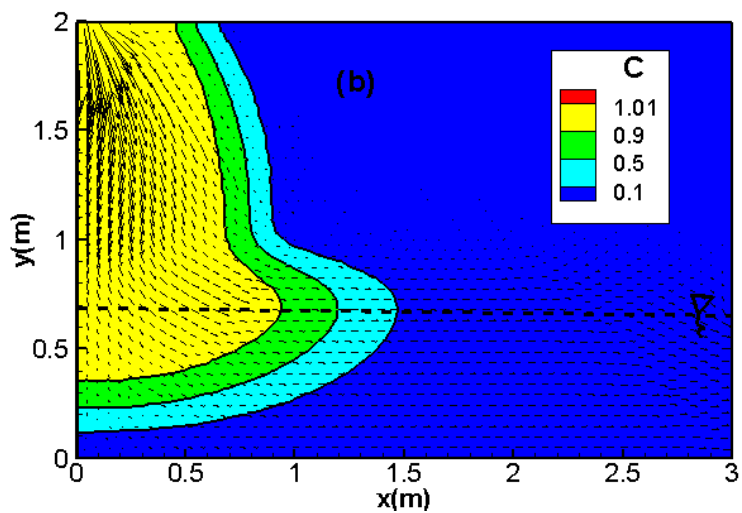
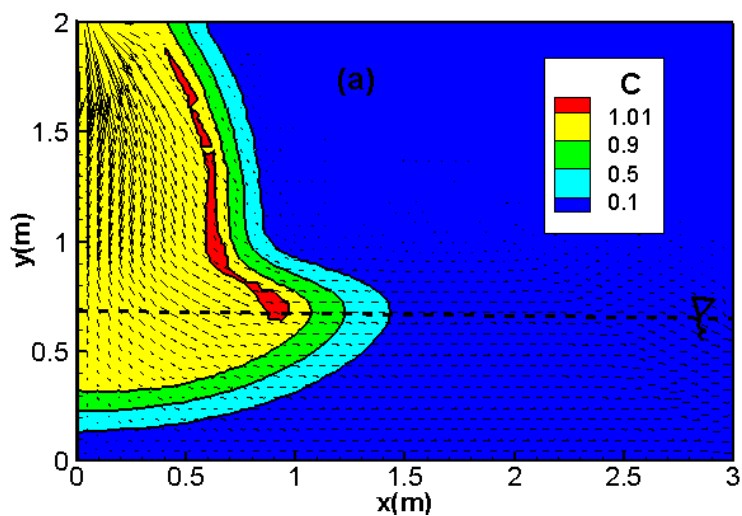


425

426 Figure 8: Concentration distribution, with the hybrid-MFE (a) and the upwind-MFE (b)  
427 schemes for the transport problem with high dispersion in a variably-saturated porous  
428 medium.

429 For the second test case with lower dispersion ( $\alpha_L = 0.01m$ ,  $\alpha_T = 0.001m$ ), the hybrid-MFE  
430 method yields unstable results containing unphysical oscillations (red color in Figure 9a).  
431 These oscillations hamper the convergence of the numerical model, and severe convergence  
432 issues can be encountered if we further decrease the dispersivity values. The results of the  
433 upwind-MFE scheme are monotone and do not contain any unphysical oscillation (Figure 9b).  
434 These results point out the robustness of the new developed upwind-MFE method for solving  
435 nonlinear multi-physics problems.





438 Figure 9: Concentration distribution with the hybrid-MFE (a) and upwind-MFE (b) methods  
439 for the transport problem with low dispersion in variably-saturated porous medium.

440



441

## 442 **5. Conclusion**

443

444 MFE is a robust numerical method well adapted for diffusion problems on heterogeneous  
445 domains and unstructured meshes. When applied to transport equations, the MFE solution can  
446 exhibit strong unphysical oscillations due to the hyperbolic nature of advection. Upwind  
447 schemes can be used to avoid such oscillations, although they introduce some numerical  
448 diffusion. In this work, we developed an upwind scheme that does not require any  
449 approximation for the upwind concentration. The method can be seen as a combination of an  
450 upwind edge/face centred FV method with the MFE method. It ensures continuity of both  
451 advective and dispersive fluxes between adjacent elements and allows to maintain the time  
452 derivative continuous, which facilitates employment of high order time integration methods  
453 via the method of lines (MOL) for nonlinear problems.

454 Numerical simulations for the transport in a saturated porous medium show that the standard  
455 hybrid-MFE method can generate unphysical oscillations due to the hyperbolic nature of  
456 advection. These unphysical oscillations are completely avoided with the new upwind-MFE  
457 scheme. The simulation of the problem of contaminant transport in a variably-saturated  
458 porous medium shows that only the upwind-MFE scheme provides a stable solution. The  
459 results point out the robustness of the developed upwind-MFE scheme when combined with  
460 the MOL for solving nonlinear transport problems.

461

462

463

464



465

## References

- 466 Belfort, B., Ramasomanana, F., Younes, A., and Lehmann, F.: An Efficient Lumped Mixed  
467 Hybrid Finite Element Formulation for Variably Saturated Groundwater Flow, 8, 352–  
468 362, <https://doi.org/10.2136/vzj2008.0108>, 2009.
- 469 Brezzi, F. and Fortin, M. (Eds.): Mixed and Hybrid Finite Element Methods, Springer New  
470 York, New York, NY, <https://doi.org/10.1007/978-1-4612-3172-1>, 1991.
- 471 Brezzi, F., Douglas, J., and Marini, L. D.: Two families of mixed finite elements for second  
472 order elliptic problems, *Numer. Math.*, 47, 217–235,  
473 <https://doi.org/10.1007/BF01389710>, 1985.
- 474 Brunner, F., Radu, F. A., and Knabner, P.: Analysis of an Upwind-Mixed Hybrid Finite  
475 Element Method for Transport Problems, *SIAM J. Numer. Anal.*, 52, 83–102,  
476 <https://doi.org/10.1137/130908191>, 2014.
- 477 Chavent, G. and Jaffré, J.: Mathematical models and finite elements for reservoir simulation:  
478 single phase, multiphase, and multicomponent flows through porous media, North-  
479 Holland; Sole distributors for the U.S.A. and Canada, Elsevier Science Pub. Co,  
480 Amsterdam; New York: New York, N.Y., U.S.A, 376 pp., 1986.
- 481 Chavent, G. and Roberts, J. E.: A unified physical presentation of mixed, mixed-hybrid finite  
482 elements and standard finite difference approximations for the determination of  
483 velocities in waterflow problems, 14, 329–348, [https://doi.org/10.1016/0309-1708\(91\)90020-O](https://doi.org/10.1016/0309-1708(91)90020-O), 1991.
- 485 Dawson, C.: Analysis of an Upwind-Mixed Finite Element Method for Nonlinear contaminant  
486 Transport Equations, 35, 1709–1724, <https://doi.org/10.1137/S0036142993259421>,  
487 1998.
- 488 Dawson, C. N. and Aizinger, V.: Upwind mixed methods for transport equations, 3, 93–110,  
489 1999.
- 490 Fahs, M., Younes, A., and Lehmann, F.: An easy and efficient combination of the Mixed  
491 Finite Element Method and the Method of Lines for the resolution of Richards’  
492 Equation, *Environmental Modelling & Software*, 24, 1122–1126,  
493 <https://doi.org/10.1016/j.envsoft.2009.02.010>, 2009.
- 494 van Genuchten, M. T.: A Closed-form Equation for Predicting the Hydraulic Conductivity of  
495 Unsaturated Soils, *Soil Science Society of America Journal*, 44, 892–898,  
496 <https://doi.org/10.2136/sssaj1980.03615995004400050002x>, 1980.
- 497 Hoteit, H., Mosé, R., Philippe, B., Ackerer, P., and Erhel, J.: The maximum principle



- 498 violations of the mixed-hybrid finite-element method applied to diffusion equations:  
499 Mixed-hybrid finite element method, 55, 1373–1390, <https://doi.org/10.1002/nme.531>,  
500 2002.
- 501 Hoteit, H., Erhel, J., Mosé, R., Philippe, B., and Ackerer, P.: Numerical Reliability for Mixed  
502 Methods Applied to Flow Problems in Porous Media, n.d.
- 503 Koohbor, B., Fahs, M., Hoteit, H., Doummar, J., Younes, A., and Belfort, B.: An advanced  
504 discrete fracture model for variably saturated flow in fractured porous media, 140,  
505 103602, <https://doi.org/10.1016/j.advwatres.2020.103602>, 2020.
- 506 Leij, F. J. and Dane, J. H.: Analytical solutions of the one-dimensional advection equation and  
507 two- or three-dimensional dispersion equation, 26, 1475–1482,  
508 <https://doi.org/10.1029/WR026i007p01475>, 1990.
- 509 Mazzia, A.: An analysis of monotonicity conditions in the mixed hybrid finite element  
510 method on unstructured triangulations, 76, 351–375,  
511 <https://doi.org/10.1002/nme.2330>, 2008.
- 512 Mualem, Y.: A new model for predicting the hydraulic conductivity of unsaturated porous  
513 media, *Water Resour. Res.*, 12, 513–522, <https://doi.org/10.1029/WR012i003p00513>,  
514 1976.
- 515 Radu, F. A., Suciu, N., Hoffmann, J., Vogel, A., Kolditz, O., Park, C.-H., and Attinger, S.:  
516 Accuracy of numerical simulations of contaminant transport in heterogeneous  
517 aquifers: A comparative study, *Advances in Water Resources*, 34, 47–61,  
518 <https://doi.org/10.1016/j.advwatres.2010.09.012>, 2011.
- 519 Raviart, P. A. and Thomas, J. M.: A mixed finite element method for 2-nd order elliptic  
520 problems, in: *Mathematical Aspects of Finite Element Methods*, Berlin, Heidelberg,  
521 292–315, 1977.
- 522 Traverso, L., Phillips, T. N., and Yang, Y.: Mixed finite element methods for groundwater  
523 flow in heterogeneous aquifers, *Computers & Fluids*, 88, 60–80,  
524 <https://doi.org/10.1016/j.compfluid.2013.08.018>, 2013a.
- 525 Traverso, L., Phillips, T. N., and Yang, Y.: Mixed finite element methods for groundwater  
526 flow in heterogeneous aquifers, *Computers & Fluids*, 88, 60–80,  
527 <https://doi.org/10.1016/j.compfluid.2013.08.018>, 2013b.
- 528 Vohralík, M.: A Posteriori Error Estimates for Lowest-Order Mixed Finite Element  
529 Discretizations of Convection-Diffusion-Reaction Equations, 45, 1570–1599,  
530 <https://doi.org/10.1137/060653184>, 2007.
- 531 Younes, A., Mose, R., Ackerer, P., and Chavent, G.: A New Formulation of the Mixed Finite



- 532           Element Method for Solving Elliptic and Parabolic PDE with Triangular Elements,  
533           149, 148–167, <https://doi.org/10.1006/jcph.1998.6150>, 1999.
- 534   Younes, A., Ackerer, P., and Lehmann, F.: A new mass lumping scheme for the mixed hybrid  
535           finite element method, *International Journal for Numerical Methods in Engineering*,  
536           67, 89–107, <https://doi.org/10.1002/nme.1628>, 2006.
- 537   Younes, A., Fahs, M., and Ahmed, S.: Solving density driven flow problems with efficient  
538           spatial discretizations and higher-order time integration methods, *Advances in Water*  
539           Resources, 32, 340–352, <https://doi.org/10.1016/j.advwatres.2008.11.003>, 2009.
- 540   Younes, A., Ackerer, P., and Delay, F.: Mixed finite elements for solving 2-D diffusion-type  
541           equations, *Rev. Geophys.*, 48, RG1004, <https://doi.org/10.1029/2008RG000277>, 2010.
- 542   Younes, A., Koohbor, B., Belfort, B., Ackerer, P., Doummar, J., and Fahs, M.: Modeling  
543           variable-density flow in saturated-unsaturated porous media: An advanced numerical  
544           model,        *Advances        in        Water        Resources*,        159,  
545           <https://doi.org/10.1016/j.advwatres.2021.104077>, 2022.
- 546
- 547